Towards a similarity theory with nonstationarity and horizontal inhomogeneity in stable atmospheric boundary layers

Marta Waclawczyk, Jun–ichi Yano, Grzegorz M Florczyk, Jackson Nzotungishaka

Graphical Abstract

Towards a similarity theory with nonstationarity and horizontal inhomgeneity in stable atmospheric boundary layers

Marta Wacławczyk, Jun-Ichi Yano, Grzegorz M. Florczyk, Jackson Nzotungishaka

Highlights

Towards a similarity theory with nonstationarity and horizontal inhomgeneity in stable atmospheric boundary layers

Marta Wacławczyk, Jun-Ichi Yano, Grzegorz M. Florczyk, Jackson Nzotungishaka

- Similarity theory for turbulence in stably stratified atmospheric boundary layers is derived by a symmetry–invariant analysis.
- The effects of both nonstationarity and horizontal inhomogeneity are included in the derived formulation.

Towards a similarity theory with nonstationarity and horizontal inhomgeneity in stable atmospheric boundary layers

Marta Wacławczyk[a], Jun-Ichi Yano[b], Grzegorz M. Florczyk[a], Jackson Nzotungishaka[a]

[a] *Faculty of Physics, University of Warsaw, Pasteura 5, Warsaw, 02-093, Poland*
[b] *CNRM, UMR3589 (CNRS), Météo France, Toulouse, 31057, France*

Abstract

Similarity functions for stably stratified atmospheric boundary layers are derived in invariant forms of the underlying system of ensemble averaged equations. Possible nonstationarity and horizontal inhomogeneity of the flows are taken into account. The analysis suggests that nonstationarity and horizontal inhomogeneity are represented through ratios of turbulence statistics. The obtained statistics by MOSAiC data analysis are found to be rather sensitive to the buoyancy frequency, nondimensionalized with the averaging time window. We propose to determine an optimal averaging time by analyzing this frequency.

Keywords:

1. Introduction

This work concerns the stably stratified atmospheric boundary layers (ABL), which form especially during the nights by surface radiative cooling. Stable stratification tends to suppress the turbulent flows with lack of buoyant energy generation. Yet, the turbulent eddies still actively transport the heat downwards. The Monin-Obukhov similarity theory (MOST) (Monin and Obukhov, 1954) describes weakly stably stratified boundary layers by adopting the Obukhov length, L, defined by a flux ratio, as the characteristic length scale. This theory assumes that all the single-point turbulence statistics, properly nondimensionalized with the use of the near-surface values of the fluxes, are universal functions of the nondimensional height, $\xi = z/L$.

However, this assumption is valid only for relatively small values with $\xi \leq 1$, i.e. with weak stratifications. With increasing stratifications, the MOST describes boundary layer less well.

Various modifications of the MOST were proposed. For example, Nieuswtadt (1984) considered the "local" Obukhov length, calculated from the fluxes measured at a given height. Sorbjan (2006, 2016) proposed to use, instead of ξ, the local Richardson number Ri as the stability parameter. Alternatively, the flux-based Richardson number was used by Łobocki (2013); Łobocki and Porretta-Tomaszewska (2021). Dependence on the Coriolis parameter and stability of free-flow were considered by Zilitinkevich and Calanca (2000), Zilitinkevich and Esau (2005, 2007). Those studies sought to derive similarity functions by using dimensional analyses, in which by identifying a set of scales for the velocity, length, temperature, etc., characteristic for a given flow, physical variables are nondimensionalized by those scales, hoping to identify universal functions.

Clearly, alternative approaches, not focusing on the dimensionalities, are desirable. Recently, Stiperski et al. (2021) took such a step by adopting the anisotropy invariant maps by Lumley and Newman (1977) developed for inhomogeneous turbulent flows, describing different states of turbulence in terms of two independent invariants of the anisotropy tensor. Stiperski and Calaf (2023) examined dependence on the turbulence anisotropy tensor to represent turbulence kinetic energy under the horizontal inhomogeneities.

Our study takes a further step of deriving those similarity functions more directly by deductively analyzing the system of governing equations of the boundary layers. More specifically, similarity functions of the governing equation system are derived solely by analyzing its mathematical symmetry, as invariant forms, without solving the equations explicitly. Here, invariant functions are those that do not change the form, *or* remain invariant under the symmetry transformations of the variables. This approach has been adopted by e.g. Oberlack (2001); Avsarkisov et al. (2014); Oberlack et al. (2022) in the context of neutral stratifications, Ji and She (2021) for ABLs using generalized dilation symmetry principle and recently for stably stratified ABLs, by Yano and Wacławczyk (2024) and Wacławczyk et al. (2024). A similar problem was addressed by Yano and Wacławczyk (2022) slightly differently with the technique of nondimensionalization (cf., Yano and Bonazzola, 2009).

This paper presents extensions of those previous analyses, especially by taking into account the spatial inhomogeneity, which has been neglected in

our previous studies. Apart from this, we address the problem of averaging time scales. Vickers and Mahrt (2003) studied the cospectral gap which separates turbulent and mesoscale contributions and argued that the averaging timescales in the stable surface layer should be small enough, to filter-out contributions from the large-scale non-turbulent motions like e.g. the internal gravity waves and drainage flows. We approach this problem in a different way, by examining the invariant forms, in order to find a criterion for the optimal averaging timescales.

2. Monin-Obukhov similarity theory

2.1. Division into the mean and eddy

In traditional ABL descriptions, all the variables are decomposed into the mean and eddies. Here, the system is never perfectly stationary with time with a well–defined single mean state, but we can define mean merely as what slowly evolves with time, and we need to approximate it by a local average:

$$\overline{f} \approx \frac{1}{T}\int_{t}^{t+T} f(t)\mathrm{d}t, \tag{1}$$

where T is an averaging timescale. This averaging, represented by overbar, filters out the small-scale eddies, and only the temporal tendencies of the "large-scale" variables are retained, as a result. By using the Reynolds decomposition, velocity and temperature are now expressed as sums of the local mean and eddy parts with the latter denoted by primes:

$$u = \overline{u} + u', \quad v = \overline{v} + v', \quad w = \overline{w} + w', \quad \theta = \overline{\theta} + \theta'. \tag{2}$$

Under this decomposition, correlations between the variables become sums of the mean parts and the eddy covariances, e.g.

$$\overline{uw} = \overline{u}\,\overline{w} + \overline{u'w'}, \quad \overline{uu} = \overline{u}\,\overline{u} + \overline{u'u'}, \quad \overline{w\theta} = \overline{w}\,\overline{\theta} + \overline{w'\theta'}. \tag{3}$$

2.2. Nondimensional vertical gradients

The Monin-Obukhov (MOST) theory remains one of the guiding principles in the studies of ABLs. It claims that the vertical structure of the ABL is characterized by a single length scale, the Obukhov scale, L, defined by

$$L = \frac{\bar{\theta}_0}{\kappa g}\frac{u_*^2}{\theta_*}, \tag{4}$$

where $\kappa = 0.4$ is the von Kármán constant, g is the gravity acceleration, $\bar{\theta}_0$ is a reference temperature (e.g. surface temperature or vertically-averaged temperature). The friction velocity u_* and temperature θ_* are calculated from the surface-values of the eddy covariances (fluxes) (i.e. measured at the lowest level, typically $z \approx 1$m) as

$$u_*^2 = -\overline{u'w'}_0, \qquad \theta_* = -\overline{w'\theta'}_0/u_*. \tag{5}$$

The nondimensonalized fluxes and mean variables can be expressed by universal similarity functions solely depending on the nondimensional height, z/L. It is observationally known that within a certain sublayer of the SBL (surface layer) where the vertical variation of fluxes $\overline{u'w'}$ and $\overline{w'\theta'}$ can be neglected, vertical gradients follow

$$\Phi_m = \frac{\kappa z}{u_*}\frac{\partial \overline{u}}{\partial z} = 1 + \beta\frac{z}{L}, \qquad \Phi_h = \frac{\kappa z}{\theta_*}\frac{\partial \overline{\theta}}{\partial z} = 1 + \beta\frac{z}{L}, \tag{6}$$

where $\beta \approx 5$. The smaller L (i.e. large $z/L \gg 1$) indicates stronger stratifications, and the gradients of $\overline{u}$ and $\overline{\theta}$ become constant, independent of height under strong stratifications. On the other hand, the larger L means that the temperature does not affect the velocity field in any significant manner. In this case, Eqs. (6) describe approximately logarithmic profiles of mean velocity and temperature.

The assumptions behind Monin-Obukhov theory are satisfied only for weak stratifications: as the degree of stratification increases, the discrepancy between the theory and observational measurements increases. Moreover, turbulence can locally collapse in the stable ABLs, and the flow becomes intermittent (laminar-turbulent). Given the high degree of complexity of flows in the stable ABLs, its representation remains an open research topic.

3. Symmetries and invariants

The "symmetry" of a differential equation is defined by a transformation of the independent and dependent variables denoted, respectively, by vectors $\mathbf{x} = (x_1, \ldots, x_m)$ and $\mathbf{y}(\mathbf{x}) = (y_1(\mathbf{x}), \ldots, y_n(\mathbf{x}))$, that do not change the form of the given equation (Bluman and Kumei, 1989). Symmetries map a solution of a given equation onto another solution of the same equation.

We will consider the continuous Lie point symmetry transformations of the form,

$$T_\epsilon : \quad \mathbf{x}^* = \mathbf{\Phi}(\mathbf{x}, \mathbf{y}; \epsilon), \quad \mathbf{y}^* = \mathbf{\Psi}(\mathbf{x}, \mathbf{y}; \epsilon), \tag{7}$$

where $\mathbf{x}^*$ and $\mathbf{y}^*$ are the transformed vector variables, and $\epsilon \in R$ is an arbitrary continuous parameter. The set of transformations (7) can be shown to fulfill the mathematical properties of a group, i.e. it contains a unitary element, an inverse element, and satisfies the closure and the associativity.

Let's take the one-dimensional heat equation (Bluman and Kumei, 1989), as an example:

$$\frac{\partial \theta}{\partial t} = \frac{\partial^2 \theta}{\partial z^2} \tag{8}$$

with the initial condition $\theta(z, 0) = \delta(z)$. They remain invariant under the following transformations of θ, z and t:

$$T_\epsilon : \quad z^* = \mathrm{e}^\epsilon z, \quad t^* = \mathrm{e}^{2\epsilon} t, \quad \theta^* = \mathrm{e}^{-\epsilon} \theta, \tag{9}$$

where $\epsilon \in R$. It can be shown that the group properties are satisfied by the transformation (9). The unitary element, T_0, exists:

$$T_0 : \quad z^* = \mathrm{e}^0 z = z, \quad t^* = \mathrm{e}^0 t = t, \quad \theta^* = \mathrm{e}^0 \theta = \theta. \tag{10}$$

Each transformation, T_ϵ, has an inverse element, $T_{-\epsilon}$:

$$T_{-\epsilon} T_\epsilon : \quad \mathrm{e}^{-\epsilon} z^* = \mathrm{e}^{-\epsilon+\epsilon} z = z, \quad \mathrm{e}^{-2\epsilon} t^* = \mathrm{e}^{-2\epsilon+2\epsilon} t = t, \quad \mathrm{e}^{\epsilon} \theta^* = \mathrm{e}^{\epsilon-\epsilon} \theta = \theta. \tag{11}$$

Furthermore, a combination of two transformations T_{ϵ_1} and T_{ϵ_2} is a new transformation $T_{\epsilon_1+\epsilon_2}$ and the associativity is satisfied as $T_{\epsilon_1}(T_{\epsilon_2} T_{\epsilon_3}) = (T_{\epsilon_1} T_{\epsilon_2}) T_{\epsilon_3}$.

The set of symmetries of a given partial differential equation can be determined by Lie group analysis. Details of this procedure are described in textbooks, e.g. Bluman and Kumei (1989), and the procedure itself is implemented in computer algebra systems.

The problem of deriving the invariant solutions of a partial differential equation system reduce to that of solving a corresponding characteristic system, which contains infinitesimal forms of the transformations. This system can be derived from the global form (7) by expanding in the Taylor series around $\epsilon = 0$:

$$\mathbf{x}^* = \mathbf{\Phi}(\mathbf{x}, \mathbf{y}; 0) + \left.\frac{\partial \mathbf{\Phi}}{\partial \epsilon}\right|_{\epsilon=0} \epsilon + \mathcal{O}(\epsilon^2), \tag{12}$$

$$\mathbf{y}^* = \mathbf{\Psi}(\mathbf{x}, \mathbf{y}; 0) + \left.\frac{\partial \mathbf{\Psi}}{\partial \epsilon}\right|_{\epsilon=0} \epsilon + \mathcal{O}(\epsilon^2). \tag{13}$$

The first term on the right-hand side both in Eqs. (12) and (13) represents the unitary element of the transformation group, hence they are equal to $\mathbf{x}$ and $\mathbf{y}$, respectively. The first–order derivatives at $\epsilon = 0$ are called "infinitesimals", and will be denoted by $\boldsymbol{\xi}$ and $\boldsymbol{\eta}$, i.e.,

$$\mathbf{x}^* = \mathbf{x} + \boldsymbol{\xi}(\mathbf{x}, \mathbf{y})\, \epsilon + \mathcal{O}(\epsilon^2), \tag{14}$$

$$\mathbf{y}^* = \mathbf{y} + \boldsymbol{\eta}(\mathbf{x}, \mathbf{y})\, \epsilon + \mathcal{O}(\epsilon^2). \tag{15}$$

The infinitesimal generator, X is defined by

$$\mathrm{X} = \boldsymbol{\xi} \cdot \nabla_{\mathbf{x}} + \boldsymbol{\eta} \cdot \nabla_{\mathbf{y}}, \tag{16}$$

where $\nabla_{\mathbf{x}}$ and $\nabla_{\mathbf{y}}$ are gradient operators with respect to $\mathbf{x}$ and $\mathbf{y}$, respectively. The solution $\mathbf{y} = \boldsymbol{\Theta}(\mathbf{x})$ is an invariant solution of the partial differential equation, if and only if it satisfies the condition:

$$\mathrm{X}\,(\mathbf{y} - \boldsymbol{\Theta}) = 0 \tag{17}$$

on $\mathbf{y} = \boldsymbol{\Theta}(\mathbf{x})$. This condition can be written in a form of a characteristic system for the components of vectors $\mathbf{x}$ and $\mathbf{y}$:

$$\frac{\mathrm{d}x_1}{\xi_1(\mathbf{x}, \mathbf{y})} = \cdots = \frac{\mathrm{d}x_m}{\xi_m(\mathbf{x}, \mathbf{y})} = \frac{\mathrm{d}y_1}{\eta_1(\mathbf{x}, \mathbf{y})} = \frac{\mathrm{d}y_2}{\eta_2(\mathbf{x}, \mathbf{y})} = \cdots = \frac{\mathrm{d}y_n}{\eta_n(\mathbf{x}, \mathbf{y})}. \tag{18}$$

Solving for the equalities in Eq. (18), we find the invariants, C_i $(i = 1, \ldots, n)$, that can now be treated as the new dependent variables with their arguments designated by X_j $(j = 1, \ldots, m-1)$. Consequently, the invariant forms read

$$C_i = F_i(X_1, X_2, \ldots, X_{m-1}), \tag{19}$$

for $i = 1, \ldots, n$, where $F_i (i = 1, \ldots, n)$ are unspecified functions.

In the following, we will derive similarity functions for the gradients of the mean velocity and temperature, the fluxes, and the correlations between velocity components in forms of invariant condition (19).

4. System of equations and its invariance under transformations of variables

4.1. System of equations

This section presents an extension of the previous symmetry analysis (Yano and Wacławczyk, 2024; Wacławczyk et al., 2024) by including the

horizontal transport. In what follows, we separate the perturbations of velocity and temperature from the reference state with the hydrostatic and geostrophic balance (e.g. Andrews, 2010), i.e.

$$\frac{\partial P}{\partial x} = \rho_0 f V, \tag{20}$$

$$\frac{\partial P}{\partial y} = -\rho_0 f U, \tag{21}$$

$$\frac{\partial P}{\partial z} = -\rho_0 g, \tag{22}$$

where f is the Coriolis parameter, U, V are the components of the geostrophic wind and ρ_0 is a reference mean density.

The effect of the Coriolis is next removed from the problem by subtracting the geostrophic–pressure balances (20), (21) from the horizontal momentum equations. As a result, only the ageostrophic component of the pressure are found in the equations. We further assume that the Coriolis terms are small and negligible close to the surface. Similarly, the hydrostatic balance equation (22) is subtracted from the full vertical momentum equation, leaving the density perturbations in the mass force term. These density perturbations are expressed in terms of the buoyancy b, using the Boussinesq approximation

$$b = -g\frac{\rho - \rho_0}{\rho_0} = g\frac{\theta - \bar{\theta}_0}{\bar{\theta}_0}, \tag{23}$$

where $\bar{\theta}_0$ is a constant reference temperature. Finally, the system is averaged using the local time average defined in Eq. (1). The local coordinate is chosen in such a manner that $\overline{v} = 0$ locally at an observational-measurement point, but in general, $\partial\overline{v}/\partial y \neq 0$ due to non-zero horizontal transport. Under these

assumptions, the governing equation system become for a "large scale":

$$\frac{\partial \overline{u}}{\partial x} + \frac{\partial \overline{v}}{\partial y} + \frac{\partial \overline{w}}{\partial y} = 0 \tag{24}$$

$$\frac{\partial \overline{u}}{\partial t} + \frac{\partial \overline{uu}}{\partial x} + \frac{\partial \overline{uv}}{\partial y} + \frac{\partial \overline{uw}}{\partial z} = -\frac{1}{\rho_0}\frac{\partial \overline{p}}{\partial x}, \tag{25}$$

$$\frac{\partial \overline{v}}{\partial t} + \frac{\partial \overline{uv}}{\partial x} + \frac{\partial \overline{vv}}{\partial y} + \frac{\partial \overline{vw}}{\partial z} = -\frac{1}{\rho_0}\frac{\partial \overline{p}}{\partial y}, \tag{26}$$

$$\frac{\partial \overline{w}}{\partial t} + \frac{\partial \overline{uw}}{\partial x} + \frac{\partial \overline{vw}}{\partial y} + \frac{\partial \overline{ww}}{\partial z} = -\frac{1}{\rho_0}\frac{\partial \overline{p}}{\partial z} + \overline{b}, \tag{27}$$

$$\frac{\partial \overline{b}}{\partial t} + \frac{\partial \overline{ub}}{\partial x} + \frac{\partial \overline{vb}}{\partial y} + \frac{\partial \overline{wb}}{\partial z} = 0, \tag{28}$$

where p is the ageostrophic and non-hydrostatic part of the pressure.

Here, the given system consists of the Navier-Stokes equations but with the zero viscosity, and additionally taking into account of the buoyancy, b. It is important to note that the Reynolds decomposition (2), discussed in Sec. 2.1, is not applied in the present system: the averages of the cross terms of the full variables are always considered, which contain both the mean and the eddy contributions. Thus, for example

$$\overline{uu} = \overline{u}\,\overline{u} + \overline{u'u'}, \quad \overline{wb} = \overline{w}\,\overline{b} + \overline{w'b'}. \tag{29}$$

This is a key difference of the present formulation from the standard convention of the eddy covariances (5). For this reason, the correlations between the instantaneous velocity components $\overline{u_i u_j}$, as well as between the velocity and the buoyancy $\overline{u_i b}$, where $i, j = 1, 2, 3$ are referred the "total fluxes" with the quotation in the following.

The system here is comparable to Eqs. (24)–(28) considered in Wacławczyk et al. (2024), but it additionally includes the mean vertical velocity $\overline{w}$, horizontal gradients $\partial/\partial x$, $\partial/\partial y$, the "total fluxes" , $\overline{uu}$, $\overline{uv}$, $\overline{vv}$, $\overline{vw}$, as well as $\overline{ub}$ and $\overline{vb}$.

4.2. Invariance of the system of equations

The goal for now is to identify the transformations of the variables that make the system (24)–(28) invariant. Those invariant transformations characterize the symmetries of the system. In seeking invariant transformations,

we consider the following types of the transformations (Pukhnachev, 1972). The first are the time and space translations:

$$t^* = t + t_0, \tag{30}$$

$$x_i^* = x_i + f_i(t), \quad {u_i}^* = u_i + \frac{\mathrm{d}f_i(t)}{\mathrm{d}t}, \quad p^* = p - x_i \cdot \frac{\mathrm{d}^2 f_i(t)}{\mathrm{d}t^2} \tag{31}$$

where $i = 1, 2, 3$, $x_1 = x$, $x_2 = y$, $x_3 = z$, and $u_1 = u$, $u_2 = v$, $u_3 = w$ denote the velocity components, $f_i(t)$ $(i = 1, 2, 3)$ are the space translation rates, which may depend on time. Further considered are the pressure translations

$$p^* = p + g(t),$$

with a space translation, $g(t)$, which may also depend on time, as well as the translations of the buoyancy and pressure

$$b^* = b + b_0, \quad p^* = p + z\rho_0 b_0. \tag{32}$$

Furthermore, the rotational invariance in the x-y plane and the scaling transformations are considered:

$$t^* = \mathrm{e}^{\alpha} t, \quad x^* = \mathrm{e}^{\beta} x, \quad y^* = \mathrm{e}^{\beta} y, \quad z^* = \mathrm{e}^{\beta} z, \tag{33}$$

$${u_i}^* = \mathrm{e}^{\beta-\alpha} u_i, \quad b^* = \mathrm{e}^{\beta-2\alpha} b, \quad p^* = \mathrm{e}^{2\beta-2\alpha}\, p, \tag{34}$$

with $\alpha, \beta \in R$ constants. Additionally, when the buoyancy force in the momentum equation (27) is negligible, the underlying system is invariant under an additional, independent scaling group $b^* = \mathrm{e}^{\epsilon} b$, with $\epsilon \in R$. For simplicity, in the following, possible time dependencies in f_i and g will be neglected, setting them to be constant of time.

Similar transformations as (30)–(34) can easily be applied to the equations (24)–(28) of the moments to identify the symmetries. For example, this system is invariant under the transformations

$$t^* = \mathrm{e}^{\alpha} t, \quad x^* = \mathrm{e}^{\beta} x, \quad y^* = \mathrm{e}^{\beta} y, \quad z^* = \mathrm{e}^{\beta} z, \tag{35}$$

$${\bar{u}_i}^* = \mathrm{e}^{\beta-\alpha} \bar{u}_i, \quad \overline{u_i u_j}^* = \mathrm{e}^{2\beta-2\alpha} \overline{u_i u_j}, \quad \overline{u_i b}^* = \mathrm{e}^{2\beta-3\alpha} \overline{u_i b}, \tag{36}$$

$$\bar{b}^* = \mathrm{e}^{\beta-2\alpha} \bar{b}, \quad \bar{p}^* = \mathrm{e}^{2\beta-2\alpha}\, \bar{p}, \tag{37}$$

where $i, j = 1, 2, 3$. The invariance of the system (24)–(28) under these transformations can be verified by direct substitutions.

As in any turbulence–closure problems treating all the moments (Reynolds stress, etc: cf. Mellor and Yamada (1974)) as *separate* variables, the present versions of "total fluxes", defined without subtracting the means, $\overline{uu}$, $\overline{vv}$, $\overline{wb}$, etc., are treated as mutually independent variables, and the resulting system (24)–(28) is linear in respect to those "total fluxes". It further suggests that equations (24)–(28) are invariant under additional scaling and translations, although they are not symmetries of the underlying Navier-Stokes system (Oberlack and Rosteck, 2010; Rosteck, 2014):

$$t^* = t, \quad x^* = x, \quad z^* = z, \quad z^* = z, \tag{38}$$

$$\bar{u}_i^* = \mathrm{e}^{\gamma}\,\overline{u_i}, \quad \bar{b}^* = \mathrm{e}^{\gamma}\,\bar{b}, \quad \overline{p}^* = \mathrm{e}^{\gamma}\,\overline{p} \tag{39}$$

$$\overline{u_i u_j}^* = \mathrm{e}^{\gamma}\,\overline{u_i u_j}, \quad \overline{u_i b}^* = \mathrm{e}^{\gamma}\,\overline{u_i b}, \tag{40}$$

where $\gamma \in R_-$ (Wacławczyk et al., 2014, 2017), and

$$t^* = t, \quad x^* = x, \quad z^* = z, \quad z^* = z, \tag{41}$$

$$\bar{u}_i^* = \overline{u_i} + u_i^0, \quad \overline{u_i u_j}^* = \overline{u_i u_j} + u_i u_j^0, \quad \overline{u_i b}^* = \overline{u_i b} + u_i b^0 \tag{42}$$

with arbitrary constants, u_i^0, $u_i u_j^0$, $u_i b^0$.

Since the transformations (39)–(42) are not symmetries of the Navier-Stokes equations, they must reflect properties of ensembles. For example, one can assume that an ensemble consists of fractional contributions from e^{γ} (≤ 1) of turbulent flow with buoyancy and $1-\mathrm{e}^{\gamma}$ of the laminar flow in which turbulence has collapsed. Then, the mean velocity and the other turbulence statistics can be written as weighted sums of these two contributions, i.e. the turbulent $\bar{u}_i^T$ and the laminar $\bar{u}_i^L$ flows:

$$\bar{u}_i = \mathrm{e}^{\gamma}\bar{u}_i^T + (1-\mathrm{e}^{\gamma})\bar{u}_i^L. \tag{43}$$

This interpretation was put forward in Wacławczyk et al. (2014). Wacławczyk et al. (2024) further argued that the scaling symmetries (39) and (40) may play a role in representing the statistics as weighted sums of neutral and buoyancy-affected contributions.

4.3. Characteristic system

In deriving the invariants of a given system, the time and space translations (30) and (31) are considered, assuming $f_i = const$, along with buoyancy and pressure translations (32), the scaling groups (33)–(34), as well as the

scaling and the translations of statistics (39), (40), and (42). As a result, the following characteristic system is obtained:

$$\frac{\mathrm{d}t}{\alpha(t-t_0)} = \frac{\mathrm{d}x}{\beta\,(x-x_0)} = \frac{\mathrm{d}y}{\beta\,(y-y_0)} = \frac{\mathrm{d}z}{\beta\,(z-z_0)} =$$
$$= \frac{\mathrm{d}\overline{u_i}}{(\beta-\alpha+\gamma)\overline{u_i}+u_i^0} = \frac{\mathrm{d}\overline{b}}{(\beta-2\alpha+\gamma)\overline{b}+b_0} = \frac{\mathrm{d}\bar{p}}{(2\beta-2\alpha+\gamma)\bar{p}+p_0+zb_0\rho_0} =$$
$$= \frac{\mathrm{d}\overline{u_iu_j}}{(2\beta-2\alpha+\gamma)\overline{u_iu_j}+u_iu_j^0} = \frac{\mathrm{d}\overline{u_ib}}{(2\beta-3\alpha+\gamma)\overline{u_ib}+u_ib^0} = \dots. \tag{44}$$

The system for the turbulence statistics (24)–(28) is not closed, so is the corresponding characteristic system (44). Adding more equations introduces the higher-order statistics, e.g. the triple correlations, fourth-order correlations, and so forth, *ad infinitum*. In spite of lack of the closure, those higher-order equations, not explicitly included in the symmetry analysis here, are also invariant under the symmetries (30)–(34), as following from the underlying, closed Navier-Stokes equation system with the additional scaling and translation (39), (40), (42), which follow from their linearity.

When the coefficients satisfy $\beta-\alpha+\gamma\neq 0$, $\beta-2\alpha+\gamma\neq 0$, $2\beta-2\alpha+\gamma\neq 0$ and $2\beta-3\alpha+\gamma\neq 0$, the solution of the system (44) consists of the following set of invariants:

$$t-t_0 = X_t\,|z-z_0|^{\tilde{\alpha}} \tag{45}$$
$$|x-x_0| = X_L\,|z-z_0| \tag{46}$$
$$|y-y_0| = X_{Tr}\,|z-z_0| \tag{47}$$
$$\overline{u_iu_j} - \widetilde{u_iu_j}^{\,0} = C_{ij}(X_t,X_L,X_{Tr})\,|z-z_0|^{2-2\tilde{\alpha}+\tilde{\gamma}}, \tag{48}$$
$$\overline{u_ib} - \widetilde{u_ib}^{\,0} = C_{bi}(X_t,X_L,X_{Tr})\,|z-z_0|^{2-3\tilde{\alpha}+\tilde{\gamma}}, \tag{49}$$
$$\bar{u}_i - \tilde{u}_i^0 = C_i(X_t,X_L,X_{Tr})\,|z-z_0|^{1-\tilde{\alpha}+\tilde{\gamma}}, \tag{50}$$
$$\frac{\bar{p}}{\rho_0} - \frac{\tilde{p_0}}{\rho_0} = C_p(X_t,X_L,X_{Tr})\,|z-z_0|^{2-2\tilde{\alpha}+\tilde{\gamma}} + \frac{\tilde{b}_0\chi[z_0-(2-2\tilde{\alpha}+\tilde{\gamma})z]}{1-2\tilde{\alpha}+\tilde{\gamma}}, \tag{51}$$
$$\bar{b} - \tilde{b}_0 = C_b(X_t,X_L,X_{Tr})\,|z-z_0|^{1-2\tilde{\alpha}+\tilde{\gamma}}, \tag{52}$$

where $\chi=(\beta-2\alpha+\gamma)/(2\beta-2\alpha+\gamma)$, $\tilde{\alpha}=\alpha/\beta$ and $\tilde{\gamma}=\gamma/\beta$; $\widetilde{u_iu_j}^{\,0}$, $\widetilde{u_ib}^{\,0}$, $\tilde{u}_i^0$ $\tilde{p_0}/\rho_0$ and $\tilde{b}_0$ are constants. We further assume that in the translations

with $\tilde{u}_i^0$ and $\widetilde{u_i u_j}^0$, only the components with $i = j = 1$ are non-zero, and we set, $\tilde{u}_1^0 = \tilde{u}^0$ and $\widetilde{u_1 u_1}^0 = \widetilde{uu}^0$. The invariants, C_{ij}, C_{bi}, C_i, C_p and C_b, are functions of X_t, X_L and X_{Tr}, and they may also depend on some characteristics, i.e., constant scales, z_0, u_*, and θ_* by dimensional consistency.

In the following two subsections, we will consider the following two limiting cases. The first considered in Sec. 4.4 is the statistically nonstationary flow with negligible horizontal transport, in which the mean variables are expected to depend on z and X_t. This is the case as considered by Wacławczyk et al. (2024), and their results will be shortly recalled. The second considered in Sec. 4.5 is the statistically stationary flow with non-negligible horizontal transports with the statistics depending on z, X_L and X_{Tr}. As it turns out, those derived functions are fairly comparable to the formulas considered by Stiperski et al. (2021); Stiperski and Calaf (2023).

4.4. Statistically nonstationary, horizontally homogeneous flow.

When the flow is horizontally homogeneous in the statistical sense, derivatives of statistics with respect to x and y are zero. Hence, in addition to $\overline{u}$, $\overline{b}$ and $\overline{p}$, only the "total fluxes", $\overline{uw}$ and $\overline{ww}$, $\overline{wb}$, are present in the system (24)–(28). Moreover, the coefficients C_{ij}, C_{bi}, C_i, C_p and C_b in Eqs. (48)–(52) depend only on X_t. If we set $\widetilde{u_1 u_3}^0 = 0$ and $\widetilde{u_3 u_3}^0 = 0$ in Eq. (48), then it follows from this equation that the ratio $\overline{uw}/\overline{ww}$ depends only on C_{13}/C_{33}, which is a function of X_t:

$$\frac{\overline{uw}}{\overline{ww}} = \frac{C_{13}(X_t)}{C_{33}(X_t)} = f(X_t) \tag{53}$$

Wacławczyk et al. (2024) further assumed that this relation can be inverted for $t - t_0$ to the vicinity of an unspecified reference time, t_0, so that X_t becomes a function of $\overline{uw}/\overline{ww}$

$$X_t = f^{-1}\left(\frac{\overline{uw}}{\overline{ww}}\right). \tag{54}$$

Alternatively, by combining Eqs. (45), (48) and (49), and inverting the relation, they obtained

$$X_t = g\left(\frac{\overline{wb}(t - t_0)}{\overline{ww}}\right), \tag{55}$$

where g is an arbitrary function.

Wacławczyk et al. (2024) focused on Eq. (54), and presented invariants, C_i and C_b, as functions of $\overline{uw}/\overline{ww}$. It leads to the following forms of the shear S and the frequency N:

$$S = \frac{d\bar{u}}{dz} = \tilde{C}_1 \left(\frac{\overline{uw}}{\overline{ww}}\right) \left(1 - \frac{z}{z_0}\right)^{\tilde{\gamma}-\tilde{\alpha}}, \tag{56}$$

$$N^2 = \frac{d\bar{b}}{dz} = \tilde{C}_b \left(\frac{\overline{uw}}{\overline{ww}}\right) \left(1 - \frac{z}{z_0}\right)^{\tilde{\gamma}-2\tilde{\alpha}}. \tag{57}$$

With this, the gradient Richardson number reads

$$Ri = \frac{N^2}{S^2} = \left(1 - \frac{z}{z_0}\right)^{-\tilde{\gamma}} \frac{\tilde{C}_b}{\tilde{C}_1^2}. \tag{58}$$

The above formula predicts that in stationary flows where $\tilde{C}_b \approx const$, $\tilde{C}_1 \approx const$ and for the case $\tilde{\gamma} = 0$, the gradient Richardson number tends to a constant value, which represents the limit of strong stratifications. However, in the presence of intermittency, the Richardson number is a function of height depending on the intermittency parameter $\tilde{\gamma}$. Wacławczyk et al. (2024) also derived the nondimensional similarity functions ϕ_m and ϕ_h, by using Eqs. (48) and (49),

$$\phi_m = \frac{\kappa z}{\sqrt{|\overline{uw}|}} \frac{\partial \overline{u}}{\partial z} = \frac{z}{\Lambda} \left(1 - \frac{z}{z_0}\right)^{\tilde{\gamma}} F\left(\frac{\overline{uw}}{\overline{ww}}\right), \tag{59}$$

$$\phi_h = \kappa z \frac{\sqrt{|\overline{uw}|}}{-\overline{wb}} \frac{\partial \bar{b}}{\partial z} = \frac{z}{\Lambda} \left(1 - \frac{z}{z_0}\right)^{\tilde{\gamma}} H\left(\frac{\overline{uw}}{\overline{ww}}\right), \tag{60}$$

where

$$\Lambda = -\frac{1}{\kappa} \frac{|\overline{uw}|^{3/2}}{\overline{wb}}. \tag{61}$$

The scale Λ defined above is akin to the local Obukhov scale by Nieuswtadt (1984). The former reduces to the latter when $\overline{w} = 0$. The local Obukhov scale is close to L in the vicinity of the surface. When $\tilde{\gamma}$ is small, the bracketed term above is close to unity, and both ϕ_m and ϕ_h depend linearly on z/Λ, which is the limit of strong stratifications in MOST. The analyses of Grachev et al. (2013) and Babić et al. (2016) show that observational data deviate from these linear predictions at strong stratifications and that these

deviations are eliminated after removing data with Ri above the threshold $Ri = 0.2$ from the database. In view of these observations, dependence on the intermittency parameter $\tilde{\gamma}$ in Eqs. (58) and (59), (60) could be related to those discrepancies, because it affects the value of Ri and causes the functions, ϕ_m and ϕ_h, to deviate from linear.

Both nondimensional functions ϕ_m and ϕ_h in Eqs. (59) and (60) also depend on $\overline{uw}/\overline{ww}$, which is expected to represent the nonstationarity because of the relation (54). Furthermore, the two variables, X_t defined by Eq. (45) and $\overline{wb}(t-t_0)/\overline{ww}$ as the argument in Eq. (55), both depend on $t - t_0$: it suggests a leading–order linear relationship between them over the time $t-t_0$:

$$X_t = \frac{(t-t_0)}{\left(1-\frac{z}{z_0}\right)^{\tilde{\alpha}}} \propto (t-t_0)\frac{\overline{wb}}{\overline{ww}}. \tag{62}$$

The term, $\overline{wb}/\overline{ww}$, has the dimension of $[s^{-1}]$, hence it can be interpreted as a buoyancy "frequency". When the flow is stationary,

$$\frac{\overline{wb}}{\overline{ww}} \propto \left(1-\frac{z}{z_0}\right)^{-\tilde{\alpha}}. \tag{63}$$

On the other hand, the invariant form Eq. (54) predicts that

$$\frac{\overline{uw}}{\overline{ww}} \propto const \tag{64}$$

for the stationary flows. Further comparison between Eqs. (63) and (64) calculated at different vertical levels may be able to draw conclusions about the characteristic scale, z_0, implicit in Eq. (64) and the coefficient, $\tilde{\alpha}$, in Eq. (63).

The similarity functions, ϕ_m and ϕ_h, now read:

$$\phi_m = \frac{z}{\Lambda}\left(1-\frac{z}{z_0}\right)^{\tilde{\gamma}} \tilde{F}\left((t-t_0)\frac{\overline{wb}}{\overline{ww}}\right), \tag{65}$$

$$\phi_h = \frac{z}{\Lambda}\left(1-\frac{z}{z_0}\right)^{\tilde{\gamma}} \tilde{H}\left((t-t_0)\frac{\overline{wb}}{\overline{ww}}\right), \tag{66}$$

and the "total fluxes" calculated from Eqs. (48) and (49) take the forms:

$$\frac{\overline{uw}}{u_*^2} = C_{13}\left((t-t_0)\frac{\overline{wb}}{\overline{ww}}\right)\left(1-\frac{z}{z_0}\right)^{2-2\tilde{\alpha}+\tilde{\gamma}}, \tag{67}$$

$$\frac{\overline{wb}}{u_* b_*} = C_{b3}\left((t-t_0)\frac{\overline{wb}}{\overline{ww}}\right)\left(1-\frac{z}{z_0}\right)^{2-3\tilde{\alpha}+\tilde{\gamma}}, \tag{68}$$

where we used the friction velocity u_* and the buoyancy scale $b_* = g\theta_*/\bar{\theta}_0$ for dimensional consistency.

The question now is how this nondimensional time, $(t-t_0)\overline{wb}/\overline{ww}$, should be interpreted. We propose to link it to the time scale, T, over which the statistics are calculated. Based on the characteristic frequency, $\overline{wb}/\overline{ww}$, the averaging time must be dynamically adjusted: the characteristic time scale of the stably–stratified boundary layer, defined in this manner, changes with time, likely fairly rapidly due to its inherent intermittency.

4.5. Statistically stationary, horizontally inhomogeneous flow.

We now turn our attention to the situations of statistical stationarity, which implies that derivatives with respect to time t in Eqs. (24)–(28) are zero, and horizontal inhomogeneity, in which the system depends on X_L and X_{Tr}, defined by Eqs. (46) and (47). On the other hand, assuming the stationary flows, dependence of the statistics on X_t drops off. As a result, the "total fluxes", and the nondimensional similarity functions now read:

$$\frac{\overline{u_i u_j}}{u_*^2} = C_{ij}(X_L, X_{Tr}) \left(1 - \frac{z}{z_0}\right)^{2-2\tilde{\alpha}+\tilde{\gamma}}, \quad (i,j) \neq (1,1), \tag{69}$$

$$\frac{\overline{uu}}{u_*^2} = C_{11}(X_L, X_{Tr}) \left(1 - \frac{z}{z_0}\right)^{2-2\tilde{\alpha}+\tilde{\gamma}} + \frac{\widetilde{uu}^0}{u_*^2}, \tag{70}$$

$$\frac{\overline{u_i b}}{u_* b_*} = C_{bi}(X_L, X_{Tr}) \left(1 - \frac{z}{z_0}\right)^{2-3\tilde{\alpha}+\tilde{\gamma}}, \tag{71}$$

$$\phi_m = \tilde{C}_1(X_L, X_{Tr}) \frac{z}{\Lambda} \left(1 - \frac{z}{z_0}\right)^{\tilde{\gamma}}, \tag{72}$$

$$\phi_h = \tilde{C}_b(X_L, X_{Tr}) \frac{z}{\Lambda} \left(1 - \frac{z}{z_0}\right)^{\tilde{\gamma}}. \tag{73}$$

In this case, it follows from Eq. (69) and (70) that the ratio of $\overline{u_i u_j}$ and kinetic energy becomes a function of X_L and X_{Tr}

$$\frac{\overline{u_i u_j} - \widetilde{uu}^0}{\overline{u_l u_l} - \widetilde{uu}^0} = \frac{C_{ij}(X_L, X_{Tr})}{C_{ll}(X_L, X_{Tr})} = F(X_L, X_{Tr}). \tag{74}$$

When the shift $\widetilde{uu}^0$ is small compared to the $\overline{u_i u_j}$, we obtain

$$\frac{\overline{u_i u_j}}{\overline{u_l u_l}} \approx F(X_L, X_{Tr}). \tag{75}$$

We now assume that relation (75) can be inverted, in such a manner that a function of X_L and X_{Tr} can be expressed by another function

$$C_{ij}(X_L, X_{Tr}) = \tilde{C}_{ij}\left(\left\{\frac{\overline{u_k u_m}}{\overline{u_l u_l}}\right\}\right), \tag{76}$$

where the curly bracket denotes a dependence on the set of components of the tensor $\overline{u_k u_m}/\overline{u_l u_l}$. Here, the indices, i and j, are added to the functions above suggesting that the forms of those functions depend on those two indices. As a result, Eq. (70) now reads:

$$\frac{\overline{uu}}{u_*^2} = \tilde{C}_{11}\left(\left\{\frac{\overline{u_k u_m}}{\overline{u_l u_l}}\right\}\right)\left(1 - \frac{z}{z_0}\right)^{2-2\tilde{\alpha}+\tilde{\gamma}} + \widetilde{uu}^0. \tag{77}$$

Intriguingly, Stiperski et al. (2021) and Stiperski and Calaf (2023) suggested a similar form for the turbulent stresses to Eq. (77) based on observational fitting:

$$\frac{\overline{u'^2}}{u_*^2} = a(\{b_{ij}\})\left(1 + 3\frac{z}{L}\right)^c, \tag{78}$$

where b_{ij} is the anisotropy defined by

$$b_{ij} = \frac{\overline{u_i' u_j'}}{\overline{u_l' u_l'}} - \frac{1}{3}\delta_{ij}. \tag{79}$$

Ansatz adopted by Stiperski et al. (2021) was that the Obukhov scale L and the friction velocity u_* are the characteristic scales to nondimenionalize the similarity forms. This suggests that $z_0 \propto -L$ in Eq. (77). Their observational data analysis further suggests that it is sufficient to consider only the dependence on the smallest eigenvalue λ_3 of the tensor, b_{ij}, so that

$$\frac{\overline{u'^2}}{u_*^2} = a(\lambda_3)\left(1 + 3\frac{z}{L}\right)^c. \tag{80}$$

rather than considering the full tensor of the form b_{ij}. Analogous formulas with the same coefficients were used for the transverse and vertical components $\overline{v'^2}$ and $\overline{w'^2}$.

Stiperski and Calaf (2023) further considered a more general case with a variable scaling coefficient, $c = c(\lambda_3)$, and found that the dependence on

anisotropy is only present in the multiplicative term $a(\lambda_3)$, while $c = const.$ This is equivalent to assuming $2 - 2\tilde{\alpha} + \tilde{\gamma} = c$ in Eq. (77). The dependence on b_{ij} in Eq. (78) is akin to the dependence on the ratio $\overline{u_i u_j}/\overline{u_l u_l}$ in Eq. (77). If we assume that $\bar{u}$ is much larger than $\bar{w}$, and $\bar{v} = 0$, then equation (77) can be rewritten as

$$\frac{\overline{u_i u_j}}{\overline{u_l u_l}} = \frac{\overline{u_i' u_j'} + \bar{u}\bar{u}\,\delta_{i1}\delta_{j1}}{\overline{u_l' u_l'} + \bar{u}\bar{u}} = \frac{\overline{u_i' u_j'}}{\overline{u_l' u_l'}} \frac{1}{1 + \frac{\bar{u}\bar{u}}{\overline{u_l' u_l'}}} + \frac{\frac{\bar{u}\bar{u}}{\overline{u_l' u_l'}}}{1 + \frac{\bar{u}\bar{u}}{\overline{u_l' u_l'}}} \delta_{i1}\delta_{j1}. \tag{81}$$

The term, $\bar{u}\bar{u}/\overline{u_l' u_l'}$, is much larger than unity, hence to the leading order

$$\frac{\overline{u_i u_j}}{\overline{u_l u_l}} \approx \frac{\overline{u_i' u_j'}}{\overline{u_l' u_l'}} \frac{\overline{u_l' u_l'}}{\bar{u}\bar{u}} + \delta_{i1}\delta_{j1}\left(1 - \frac{\overline{u_l' u_l'}}{\bar{u}\bar{u}}\right) = (b_{ij} + \frac{1}{3}\delta_{ij} - \delta_{i1}\delta_{j1}) \frac{\overline{u_l' u_l'}}{\bar{u}\bar{u}} + \delta_{i1}\delta_{j1}. \tag{82}$$

The above formula contains b_{ij}, but also the ratio of turbulent to mean kinetic energy $\overline{u_l' u_l'}/\bar{u}\bar{u}$. We expect that this ratio decreases to zero when the flow re-laminarises. Hence, $\overline{u_l' u_l'}/\bar{u}\bar{u}$ can be understood as a correction for the intermittency of the flow.

5. Data and methods

5.1. Measurement data

The MOSAiC expedition was conducted between October 2019 and October 2020 on the icebreaker RV Polarstern. The MOSAiC camp was established on an ice floe in October 2019 and drifted 3400 km on a zigzagging course in the Arctic, reaching 88°36' North. A large set of measurement data was collected during the expedition on the ice surrounding the ship by monitoring stations, drifting as far as 50 km from Polarstern, research balloons, drones, and helicopter flights. High frequency observations of wind velocity and temperature at the sampling rates of 10 Hz were performed by ultrasonic anemometers mounted on meteorological tower with sensors at 2, 6, and 10 m above the initial snow/ice surface (Cummins et al., 2023). MOSAiC was the longest ever expedition in the central Arctic, with the total of 442 scientific and technical staff members, who traveled to RV Polarstern throughout the year.

This study uses raw data for wind velocity and temperature from the meteorological tower, available on open database (Cox et al., 2023). A period

of 3 December 2019 to 12 December 2019 is selected: over this period, the conditions rapidly changed from near-neutral to strongly stratified.

5.2. Methods

Time series of velocity and temperature fields were first post-processed to remove standalone spikes and replaced them with a linear interpretation of the two adjoining temporal measurements. Spikes were defined as measurements that deviates from the local thirty-minutely average by the three standard deviations. Data were analyzed with Matlab tools.

In estimating the turbulence statistics, the x direction is taken as that of the mean flow, y as the transverse, and z as the vertical. In this coordinate system, the longitudinal, horizontal-transverse and vertical velocity components u, v, and w, were calculated.

In order to calculate eddy covariances, we used 1min window for detrending the data, as such time was estimated as optimal for stable BLs by Vickers and Mahrt (2003) and by Stiperski and Calaf (2023). Next, the turbulent fluxes were additionally averaged over 10-min window for a better convergence of statistics.

For the estimation of the "total fluxes", data were not detrended, however, in order to reduce the effect of non-turbulent inertial oscillations on the local Obukhov scale Λ, we used a high pass filter and removed low-frequency oscillations of the vertical velocity, using the cut-off time scale of 1h. The correlations $\overline{uw}$, $\overline{ww}$ and $\overline{ww}$ were calculated using instantaneous variables, with the averaging window of 1 min.

6. Results

Time series of velocity at levels $z = 2$ m and $z = 6$ m, buoyancy flux as well as the turbulence kinetic energy at $z = 2$ m for selected 10 days are presented in Fig. 1. Initially (up to $t \approx 70$ h) winds are strong and the conditions are close to neutral, but with a decaying tendency of the turbulence. Winds become stronger again later at $t \approx 120$h yet the BL remains stably stratified.

We first investigate the similarity functions (63) and (64). The first one suggests that the ratio of the "total fluxes" $\overline{wb}/\overline{ww}$ might depend on height even if the flow is stationary, while the latter predicts $\overline{uw}/\overline{ww} \approx const$ under the stationarity. Time series presented in Figs. 2 and 3 support these

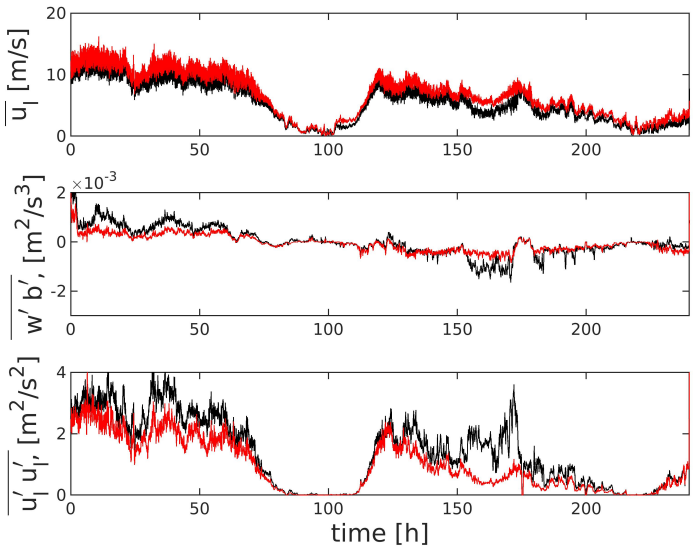

Figure 1: Time series of mean velocity $\bar{u}$, mean buoyancy flux $\overline{w'b'}$ and the turbulence kinetic energy $2k = \overline{u_l'u_l'}$ at level $z = 2$m (black line) and at $z = 6$m (red line).

predictions. We selected 20h of measurements, $t \in [105, 125]$h, where conditions changed from strongly nonstationary to stationary and zoomed 1 hour $t \in [114, 115]$h. Time series measured at $z = 2$m and $z = 6$m were compared. The ratio $\overline{wb}/\overline{ww}$ presented in Fig. 2 changes with height even when the flow is stationary. Is is negative close to the surface and changes sign to positive at $z = 6$m. The ratio $|\overline{uw}|/\overline{ww}$ varies in time mostly for $t \in [105, 110]$h, and difference between time series measured at $z = 2$m and $z = 6$m is visible for this period. The measured values at both heights become comparable later, as predicted by Eq. (64).

Next, we will compare the two forms of the nondimensional function ϕ_m, which follow from the symmetry theory. The similarity forms (48)–(52) suggest that all the statistics generally depend on the same component $|z - z_0|$. By comparing Eq. (48) with the empirical formula (78), we conclude $z_0 \propto -L$, such that

$$\left(1 - \frac{z}{z_0}\right)^{2-2\tilde{\alpha}+\tilde{\gamma}} \propto \left(1 + 3\frac{z}{L}\right)^{c} = (1 + 3\xi)^c. \tag{83}$$

Then, also other statistics will depend on $(1 + 3\xi)$, as follows from the in-

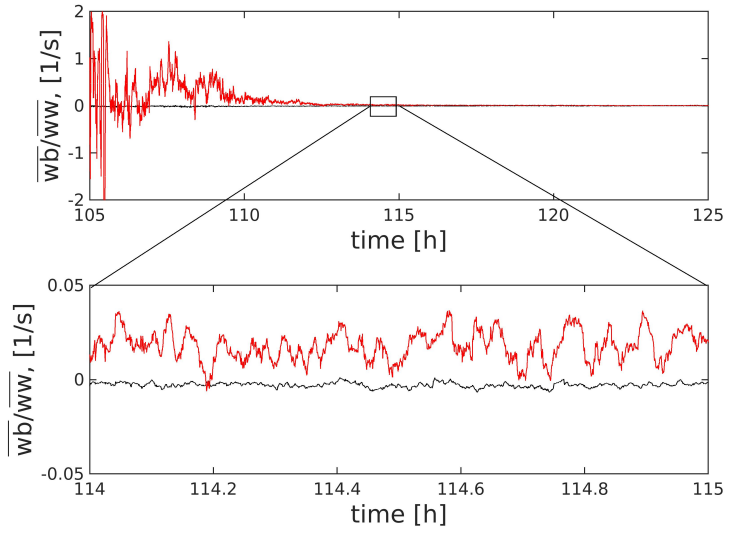

Figure 2: Time series of $\overline{wb}/\overline{ww}$ at level $z = 2$m (black line) and at $z = 6$m (red line).

variant forms (48)–(52), in particular Eq. (59) can also be rewritten as

$$\phi_m \propto \xi \left(1 + 3\xi\right)^{\tilde{\gamma}} F\left(\frac{\overline{uw}}{\overline{ww}}\right), \tag{84}$$

where we have additionally assumed that $\Lambda \approx L$ and $z/\Lambda \approx \xi$ relatively close to the ground.

As pointed out by several authors (e.g. Kim, 1999; Hicks, 1978), when ϕ_m is plotted as a function of ξ, spurious self-correlations might appear due to the common divisor u_*, present in the definition of the Obukhov scale (4) and in the definition of the non-dimensional gradient ϕ_m in Eq. (6). Klipp and Mahrt (2004) suspected that the scaling of ϕ_m observed at strong stratifications could result from the self-correlations.

In order to avoid self-correlations, instead of ϕ_m we calculated the function $\phi_m \phi_w^{-1}$ defined as

$$\phi_m \phi_w^{-1} = \left(\frac{\kappa z}{\sqrt{|\overline{uw}|}} \frac{\partial \bar{u}}{\partial z}\right) \left(\frac{\sqrt{|\overline{uw}|}}{\sqrt{\overline{w^2}}}\right) = \frac{\kappa z}{\sqrt{|\overline{w^2}|}} \frac{\partial \bar{u}}{\partial z}, \tag{85}$$

(cf. Babić et al., 2016). With this definition, no common divisor exists in the non-dimensional gradient and its variable $\xi = z/\Lambda$.

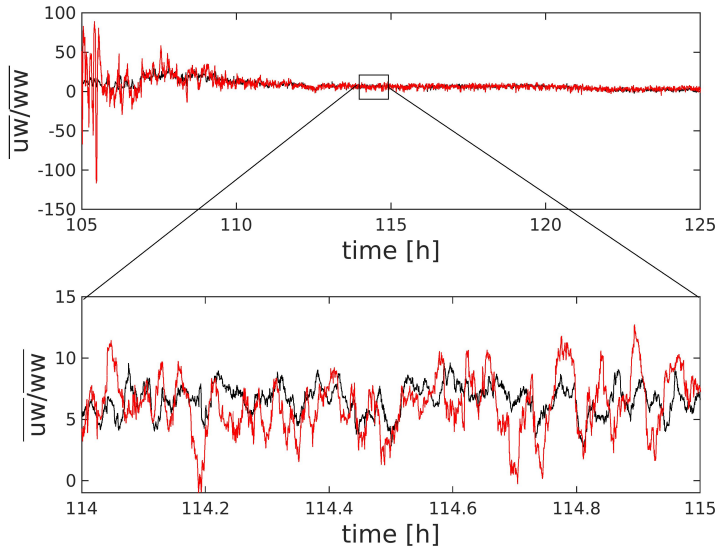

Figure 3: Time series of $|\overline{uw}|/\overline{ww}$ at level $z = 2$m (black line) and at $z = 6$m (red line).

Figs. 4–6 compare the MOSAiC data for the period 3–12 December 2019 with the theoretical predictions at three levels, $z = 2$m, $z = 6$m and $z = 10$m, respectively. The black line in Figs. 4–6 represents the log-linear prediction $\phi_m \phi_w^{-1} = 1 + a\xi$. We note that unlike in the conventional ABL studies, we do not use the Reynolds decomposition and the variables are non-dimensionalized with the "total fluxes" instead of the eddy covariances, see Eqs. (59)–(61). Hence, the constants in the scaling laws might be different than those used in MOST. In Figs. 4–6 the best fit was obtained for $a = 20$. The alternative function $\phi_m \phi_w^{-1} = 1 + b\xi\,(1 + 3\xi)^{\tilde{\gamma}}$ (dashed line) is defined by Eq. (84). The unity is added to account for neutral stratification. The latter is plotted with $b = 15$ and $\tilde{\gamma} = -1$, where the non-zero $\tilde{\gamma}$ represents the intermittency. Some data clearly deviate from the log-linear prediction at large ξ, in agreements with analyses by other authors. This discrepancy is attributed to the $|\overline{uw}|/\overline{ww}$-dependence of ϕ_m with the largest deviations from the similarity curves associated with small $|\overline{uw}|/\overline{ww}$, as shown by colors in Figs. 4a–6a: for a better collapse of the data, this dependence must be taken into account. The corresponding results for ϕ_h are inconclusive due to large measurement uncertainties, especially at low stratifications. Therefore, the analysis of ϕ_h is left for future work.

We next investigated formula (65), interpreting $t - t_0$ as the averaging window T

$$\phi_m \propto \xi \left(1 + 3\xi\right)^{\tilde{\gamma}} \tilde{F} \left(\frac{\overline{wb}}{\overline{ww}} T \right). \tag{86}$$

We used a constant averaging window $T = 1$ min. The results are presented in Figs. 4b–6b. The results are scattered, however this scatter could be reduced by specifying $\tilde{F}$ in Eq. (86).

In order to find averaging window, which satisfies the condition $(|\overline{wb}|/\overline{ww})T \sim \mathcal{O}(1)$, we plotted time series of the period T_b defined as

$$T_b = \frac{\overline{ww}}{|\overline{wb}|} \tag{87}$$

in Fig. 7 and compared it to the Brunt-Väisälä period $T_N = 1/N = (\partial\bar{b}/\partial z)^{-1}$. The local gradient Richardson number is plotted also in parallel in Fig. 7. The time scale T_b is of the order 100s for small Richardson numbers. However, as Ri increases, T_b becomes considerably smaller, and becomes comparable to, or smaller than the Brunt-Väisälä period T_N.

This suggests that smaller averaging windows are more preferable with associated high-frequency buoyancy variabilities, and the condition of $(|\overline{wb}|/\overline{ww})T \sim \mathcal{O}(1)$ could be used, either to set the averaging window for the data under study or to dynamically change T.

7. Conclusions

In this study, we investigated the similarity functions derived from the equation system for turbulence statistics. The invariant forms (45)–(52) have been derived from the symmetries of the Navier-Stokes equations. This procedure has identified a new set of independent variables. One of them, X_t, depends on time and height z, and the other two, X_L and X_{Tr}, depend on spatial constraints. Furthermore, the two limiting cases have been considered: the nonstationary, horizontally homogeneous flow, in which the statistics depend only on X_t and z, and the stationary flow with horizontal inhomogeneities, in which the statistics depend on X_L, X_{Tr} and z.

Analyzing the invariant forms, the dependence on X_t has been replaced by that on the ratio of fluxes $|\overline{uw}|/\overline{ww}$, or alternatively on the nondimensional time $|\overline{wb}|/\overline{ww}T$, in which we interpret T as the averaging time. The

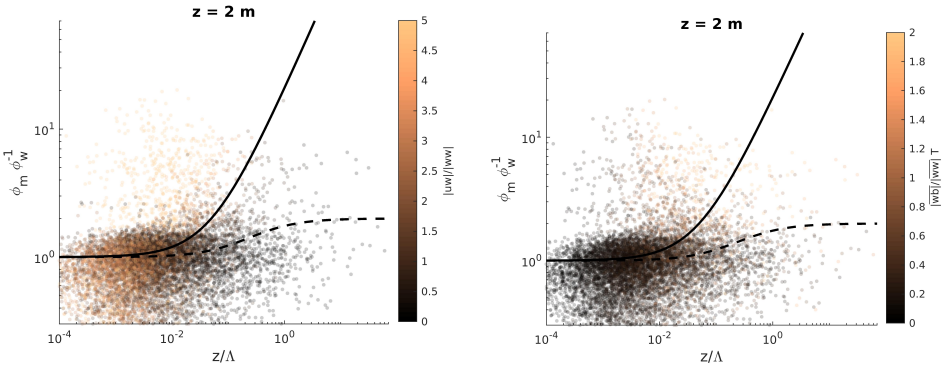

Figure 4: Similarity function ϕ_m as a function of ξ for 1 min averaging window at $z = 2$m. MOST predictions $\phi_m = 1 + a\xi$ are denoted by black solid line, formula $\phi_m = 1 + b\xi\,(1 + 3\xi)^{\tilde{\gamma}}$ which follows from Eq. (86) is presented as a black dashed line: color coded by a) the ratio $|\overline{uw}|/\overline{ww}$ and b) $T|\overline{wb}|/\overline{ww}$.

obtained similarity functions suggest that $|\overline{uw}|/\overline{ww}$ remains constant with height in stationary flows, while $|\overline{wb}|/\overline{ww}$ can change with height, even under stationarity.

Our analysis of the MOSAiC data support these predictions. The data analysis especially suggests that the condition $T|\overline{wb}|/\overline{ww} \sim \mathcal{O}(1)$ is required as a proper averaging time. Alternatively, the averaging time must be changed dynamically with time. Scatters of dependencies of ϕ_m on both $|\overline{uw}|/\overline{ww}$ or $(|\overline{wb}|/\overline{ww})T$ could be reduced by choosing an optimal averaging time.

Analyses of horizontal transports are left for future work. We expect that the "total fluxes" $\overline{uv}$ and $\overline{vw}$ are related to the horizontal gradients of velocity through the gradient diffusion hypothesis. We also plan to verify the derived formulas against larger sets of data, including those from different measurement sites.

Acknowledgements

This research was funded by the National Science Centre, Poland grant number 2020/37/B/ST10/03695, through the OPUS 19 program.

Data used in this manuscript were produced as part of the international Multidisciplinary drifting Observatory for the Study of Arctic Climate (MOSAiC) expedition with tag MOSAiC20192020. We also thank all persons

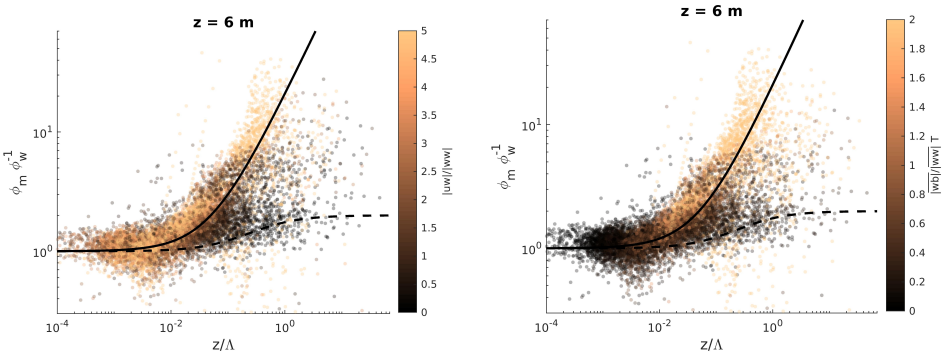

Figure 5: Similarity function ϕ_m as a function of ξ for 1 min averaging window at $z = 6$m. MOST predictions $\phi_m = 1 + a\xi$ are denoted by black solid line, formula $\phi_m = 1 + b\xi\,(1 + 3\xi)^{\tilde{\gamma}}$ which follows from Eq. (86) is presented as a dashed black line: color coded by a) the ratio $|\overline{uw}|/\overline{ww}$ and b) $T|\overline{wb}|/\overline{ww}$.

involved in the expedition of the Research Vessel Polarstern during MOSAiC in 2019—2020 (AWI_PS122_00) as listed in Nixdorf et al. (2021).

References

Andrews, D. G. 2010. An Introduction to Atmospheric Physics, Cambridge University Press, Cambridge.

Avsarkisov, V., Hoyas, S., Oberlack, M. and García-Galache, J., 2014. Turbulent plane Couette flow at moderately high Reynolds number. Journal of Fluid Mechanics 751 R1.

Babić, K., Rotach, M. W., Klaić, Z. B., 2016. Evaluation of local similarity theory in the wintertime nocturnal boundary layer over heterogeneous surface. Agric. For. Meteorol., 228-229 164–179.

Bluman, G. W., Kumei, S., 1989. Symmetries and Differential Equations. Springer–Verlag, New York.

Cummins, D. P., Guemas, V., Cox, C. J., Gallagher, M. R., Shupe, M. D., 2023. Surface turbulent fluxes from the MOSAiC campaign predicted by machine learning. Geophys. Res. Lett. 50, e2023GL105698.

Cox, C., Gallagher, M., Shupe, M. D., Persson, O., Blomquist, B., Grachev, A., et al., 2023. Met city meteorological and surface flux

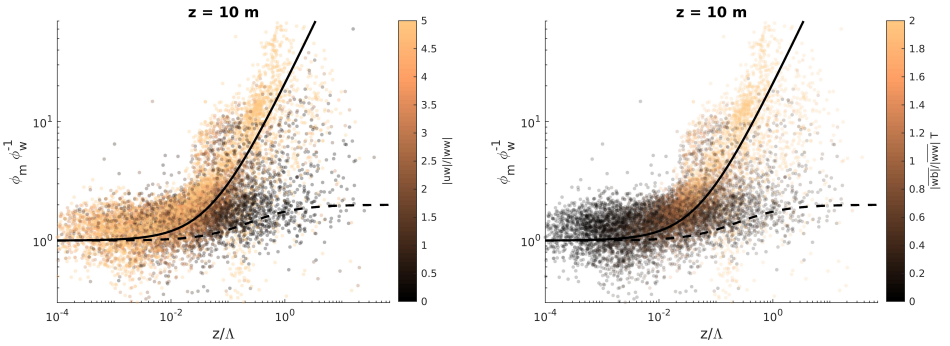

Figure 6: Similarity function ϕ_m as a function of ξ for 1 min averaging window at $z = 10$m. MOST predictions $\phi_m = 1 + a\xi$ are denoted by black line, formula $\phi_m = 1 + b\xi\,(1 + 3\xi)^{\tilde{\gamma}}$ which follows from Eq. (86) is presented as a dashed red line: color coded by a) the ratio $|\overline{uw}|/\overline{ww}$ and b) $T|\overline{wb}|/\overline{ww}$.

measurements (level 3 final), multidisciplinary drifting observatory for the study of Arctic climate (MOSAiC), central Artic, October 2019 - September 2020 [Dataset]. NSF Arctic Data Center. Available online: https://doi.org/10.18739/A2TM7227K (accessed on 28 12 2024).

Grachev, A. A., Andreas, E.L., Fairall, C.W. et al., 2013. The Critical Richardson Number and Limits of Applicability of Local Similarity Theory in the Stable Boundary Layer. Boundary-Layer Meteorol 147, 51–82.

Hick, B. B., 1978. Some limitations of dimensional analysis and power laws. Boundary-Layer Meteorol 14, 567–569.

Ji, Y., She, Z.S., 2021. Analytic derivation of Monin-Obukhov similarity function for open atmospheric surface layer. Sci. China Phys. Mech. Astron. 64, 34711.

Kim, J. H., 1999. Spurious correlation between ratios with a common divisor. Stat. Probabil. Lett. 44, 383–386.

Klipp, C. L., Mahrt, L., 2004. Flux–gradient relationship, self-correlation and intermittency in the stable boundary layer. Q. J. R. Meteorol. Soc. 130, 2087–2103.

Lumley, J., Newman, G., 1977. The return to isotropy of homogenous turbulence. J. Fluid Mech. 82, 161–178.

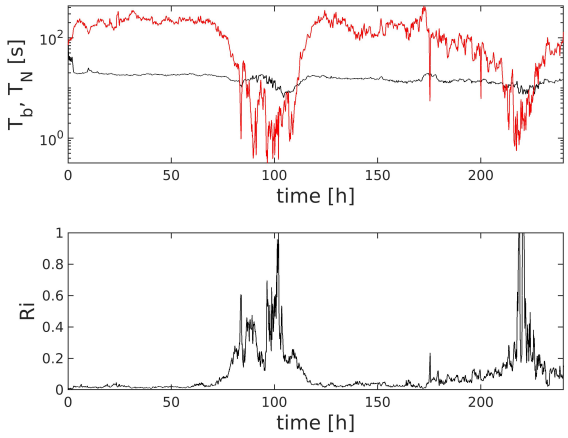

Figure 7: Upper plot: the buoyancy period T_b defined in Eq. (87) – red line, the Brunt-Väisälä period $T_N = 1/N = (\partial\bar{b}/\partial z)^{-1}$ – black line, lower plot: the Richardson number Ri for level $z = 2$m as a function of time.

Łobocki, L., 2013. Analysis of vertical turbulent heat flux limit in stable conditions with a local equilibrium, turbulence closure model. Boundary-Layer Meteorol. 148 541–555.

Łobocki, L., Porretta-Tomaszewska, P., 2021. Prediction of gradient-based similarity functions from the Mellor–Yamada model. Q J R Meteorol Soc 147, 3922–3939.

Mellor G. L., Yamada T., 1974. A Hierarchy of Turbulence Closure Models for Planetary Boundary Layers. J. Atmos. Sci. 31, 1791–1806.

Monin, A.S., Obukhov, A.M., 1954. Basic laws of turbulent mixing in the surface layer of the atmosphere. Tr. Nauk SSSR Geophiz. Inst.24, 163–187 (in Russian: translation available at: https://mcnaughty.com/keith/papers/Monin_and_Obukhov_1954.pdf)

Nieuswtadt, F.T.M., 1984. The turbulent structure of the stable, nocturnal boundary layer. Journal Atmos. Sci. 41, 2202–2216.

Nixdorf, U. et al., 2021. MOSAiC Extended Acknowledgement. Zenodo. Available online: https://doi.org/10.5281/zenodo.5179738412 (accessed on 14 01 2025).

Oberlack, M., 2001. A unified approach for symmetries in plane parallel turbulent shear flows. Journal of Fluid Mechanics 427, 299–328.

Oberlack, M., Rosteck, A., 2010. New statistical symmetries of the multipoint equations and its importance for turbulent scaling laws. Discrete and Continuous Dynamical Systems - S 3, 451–471.

Oberlack, M., Hoyas, S., Kraheberger, S. V., Alcántara–Ávila, F., Laux, J., 2022. Turbulence statistics of arbitrary moments of wall–bounded shear flows: A symmetry approach. Phys. Rev. Lett. 128, 024502.

Peng, S., Yang, Q., Shupe, M. D., Han, B., Chen, D., Liu, C., 2024. The vertical structure of turbulence kinetic energy near the Arctic sea-ice surface. Geophys. Res. Lett. 51, e2024GL110792.

Pukhnachev, V. V., 1972. Invariant solutions of Navier-Stokes equations describing motions with free boundary. Dokl. Akad. Nauk 202, 302.

Rosteck, A., 2014. Scaling Laws in Turbulence – A Theoretical Approach Using Lie-Point Symmetries. PhD Thesis, TU Darmstadt, Germany.

Schiavon, M., Barbano, F., Brogno, L. et al., 2023. On the parametrizations for the dissipation rate of the turbulence kinetic energy in stable conditions. Bull. of Atmos. Sci.& Technol. 4, 3.

Stiperski, I., Chamecki, M. and Calaf, M. 2021. Anisotropy of Unstably Stratified Near-Surface Turbulence. Boundary-Layer Meteorol 180, 363–384

Stiperski, I. and Calaf, M. 2023. Generalizing Monin-Obukhov Similarity Theory (1954) for Complex Atmospheric Turbulence. Phys. Rev. Lett. 130, 124001.

Sorbjan, Z., 2006. Local structure of stably stratified boundary layer. Journal Atmos. Sci. 63, 1526–1537.

Sorbjan, Z., 2016. Similarity scaling system for stably stratified turbulent flows. Q. J. Royal Meteorol. Soc. 142, 805–810.

Vickers, D., Mahrt, L., 2003. The Cospectral Gap and Turbulent Flux Calculations. J. Atmos. Oceanic Technol., 20, 660–672.

Wacławczyk, M., Staffolani, N., Oberlack, M., Rosteck, A., Friedrich, R., 2014. Statistical symmetries of the Lundgren–Monin–Novikov hierarchy. Phys. Rev E 90, 023022-1–11.

Wacławczyk, M., Grebenev, V. N., Oberlack, M., 2017. Lie symmetry analysis of the Lundgren-Monin-Novikov equations for multi-point probability density functions of turbulent flow. J. Phys. A: Math. Theor. 50, 175501

Wacławczyk, M., Yano, J.-I., Florczyk, G. M., 2024. Local similarity theory as the invariant solution of the governing equations. Boundary-Layer Meteorol. 190, 23.

Yano, J.I., Bonazzola, M., 2009. Scale analysis for large-scale tropical atmospheric dynamics. J. Atmos. Sci. 66, 159–172.

Yano, J.-I., Wacławczyk, M., 2022. Nondimensionalization of the Atmospheric Boundary-Layer System: Obukhov Length and Monin–Obukhov Similarity Theory. Boundary-Layer Meteorol 182, 417–439.

Yano, J.-I., and Wacławczyk, M., 2024. Symmetry Invariant Solutions in Atmospheric Boundary Layers J. Atmos. Sci., 81, 263–277.

Zilitinkevich, S., Calanca, P., 2000. An extended similarity–theory for the stably stratified atmospheric surface layer. Q. J. Royal Meteorol. Soc. 126, 1913–1923.

Zilitinkevich, S., Esau, I.G., 2005. Resistance and heat–transfer for stable and neutral planetary boundary layers: Old theory advanced and re–evaluated. Q. J. Royal Meteorol. Soc. 131, 1863–1892.

Zilitinkevich S., Esau, I.G., 2007. Similarity theory and calculation of turbulent fluxes at the surface for the stably stratified atmospheric boundary layer. Boundary-Layer Meteorol. 125, 193–205.